Pacific Northwest National Laboratory
Operated by Battelle for the
U.S. Department of Energy

Assessment of Current Process Modeling Approaches to Determine Their Limitations, Applicability and Developments Needed for Long-Fiber Thermoplastic Injection Molded Composites

BN Nguyen   RE Norris
J Holbery   J Phelps
MT Smith   CL Tucker III
V Kunk

November 2006

Property Prediction Tools for Tailored Polymer Composite Structures:

Assessment of Current Process Modeling Approaches to Determine Their Limitations, Applicability and Developments Needed for Long-Fiber Thermoplastic Injection Molded Composites

Ba Nghiep Nguyen, James D Holbery, and Mark T Smith
Pacific Northwest National Laboratory

Vlastimil Kunc and Robert E. Norris
Oak Ridge National Laboratory

Jay Phelps and Charles L. Tucker III
University of Illinois at Urbana-Champaign

Pacific Northwest National Laboratory
Operated by Battelle for the U.S. Department of Energy

OAK RIDGE NATIONAL LABORATORY
Managed by UT-Battelle for the Department of Energy

Contents

1. Introduction

Recently, long-fiber injection molded thermoplastics (LFTs) have generated great interest within the automotive industry as these materials can be used for structural applications in order to reduce vehicle weight. However, injection-molding of these materials poses a great challenge because of two main reasons: (i) no process models for LFTs have been developed that can be used to predict the processing of an LFT part, and (ii) no experimental characterization methods exist to fully characterize the as-formed LFT microstructure to determine the fiber orientation and length distributions and fiber dispersion that are critical for any process model development.

This report describes the status of the current process modeling approaches to predict the behavior and flow of fiber-filled thermoplastics under injection molding conditions. Previously, models have been developed to simulate the injection molding of short-fiber thermoplastics. The microstructure resulting from the constituents' material properties and characteristics as well as processing parameters can then be predicted for an as-formed composite part or component. Our objective is to assess these models in order to determine their capabilities and limitations, and the developments needed for long-fiber injection-molded thermoplastics.

First, the concentration regimes are summarized to facilitate the understanding of different types of fiber-fiber interaction that can occur for a given fiber volume fraction [1]. After the formulation of the fiber suspension flow problem and the simplification leading to the Hele-Shaw approach e.g. [2], the interaction mechanisms are discussed. Next, the establishment of the rheological constitutive equation is presented that reflects the coupled flow/orientation nature [1, 3]. The decoupled flow/orientation approach is also discussed which constitutes a good simplification for many applications involving flows in thin cavities. Finally, before outlining the necessary developments for LFTs, some applications of the current orientation model [4-6] and the so-called modified Folgar-Tucker model [7-8] are illustrated through the fiber orientation predictions for selected LFT samples.

2. Concentration regimes

The concentration regimes can be defined in terms of the fiber aspect ratio $r = l/d$ (where l and d are the fiber length and diameter, respectively). Basically, there are three concentration regimes which are the dilute, semi-concentrated (or semi-dilute), and concentrated regimes [1]. A suspension is dilute only if the concentration:

$$c << \frac{1}{r^2} \tag{1}$$

This requirement can also be expressed in terms of the density number (particles per unit volume) as:

$$n << \frac{1}{l^3} \tag{2}$$

The semi-concentrated regime is determined by:

$$\frac{1}{r^2} << c << \frac{1}{r} \quad \text{or} \quad \frac{1}{l^3} << n << \frac{1}{l^2 d}, \tag{3}$$

and the concentrated regime is attained if:

$$c > \frac{1}{r} \quad \text{or} \quad n > \frac{1}{l^2 d}. \tag{4}$$

In long-fiber systems the average fiber aspect ratio is about 100 or higher. This means that a suspension with a volume fraction higher than 1% is already considered as concentrated. Composites for structural applications typically possess volume fractions about 20% or higher. This illustrates the highly challenging nature of the problem to be addressed: *modeling flow of a non-dilute long fiber suspension in a non-Newtonian solvent.*

3. Problem formulation

A typical injection molding process comprises three-steps: mold filling, packing and holding, and cooling. Filling is of greater importance in injection molding of fiber-reinforced thermoplastics since the fiber orientation in different sections of the part is almost entirely determined by the flow patterns during filling. The flow of a suspension under non-isothermal and incompressible conditions obeys the following equations from continuum mechanics e.g. [9]:

Balance of mass:
$$\frac{\partial u_i}{\partial x_i} = 0, \tag{5}$$

Balance of momentum:
$$\rho(\frac{\partial u_i}{\partial t} + u_j \frac{\partial u_i}{\partial x_j}) = -\frac{\partial P}{\partial x_i} + \frac{\partial \tau_{ji}}{\partial x_j}, \tag{6}$$

Balance of energy:
$$\rho c_{\mathrm{p}} (\frac{\partial T}{\partial t} + u_i \frac{\partial T}{\partial x_i}) = k \frac{\partial}{\partial x_j} (\frac{\partial T}{\partial x_j}) + \tau_{ij} \dot{\gamma}_{ij}. \tag{7}$$

where u_i is the velocity, ρ is the density, c_{p} is the specific heat, k is the thermal conductivity, P is the pressure, τ_{ij} is the extra stress (see definition in Section 6), and $\dot{\gamma}_{ij}$ is the strain rate. The following assumptions are made: *(i) the mold is thin (thickness is much smaller than other characteristic dimensions), (ii) inertia effects are negligible, and (iii) the fluid is generalized Newtonian*. In addition to these equations, the *constitutive equation* for a suspension of fibers in a suspending fluid and the *fiber orientation equation* must be specified. The governing equations can be solved using a numerical method (e.g. a finite element method) with associated boundary conditions. Simplifications are also needed to treat practical engineering problems. The next section reviews an important approximation leading to the generalized Hele-Shaw model.

4. The generalized Hele-Shaw approach

The modeling of transient flow during the filling stage uses a generalized quasi-steady state Hele-Shaw flow model that is based on lubrication approximations (e.g. [2,10]). Basically, these approximations are used to reduce the fully 3-D flow problem (Equation (6)) to a two-

dimensional one for the pressure. Accordingly, simplifications brought to the balance of momentum equation lead to

$$\frac{\partial}{\partial x_i}\left(S\frac{\partial P}{\partial x_i}\right)=0 \qquad (8)$$

where S is the measure of the ease with which the fluid flows locally and is given by:

$$S=\int_0^h \frac{z^2 dz}{\eta} \qquad (9)$$

in which z is the gap-wise direction, h is the half gap that can be a function of the in-plane coordinates, and η is the viscosity of the fluid. Once, Equation (8) has been solved for the pressure, the average velocity components across the gap are determined by:

$$\bar{u}_i = \frac{-S}{h}\frac{\partial P}{\partial x_i} \qquad (10)$$

The velocity components will be used in the fiber orientation equation. The next section analyzes the interaction mechanisms in order to understand how they affect the fiber orientation. The Advani-Folgar-Tucker [4-5] fiber orientation equation and a modified form of this equation will then be presented. Section 6 will focus on the rheological constitutive equation.

5. Fiber-fiber interactions and fiber orientation equation

In dilute suspensions where the fiber-fiber interaction is quasi absent or negligible, the fibers orient according to the Jeffrey equation [11]. However, the concentrations for practical engineering applications are not dilute, and the fiber-fiber interaction mechanisms play an essential role in controlling the fiber orientation. In general, fiber-fiber interactions can be classified into two categories: *hydrodynamic interaction* [12] and *mechanical interaction* [13], [14]. Hydrodynamic interactions are hydrodynamic in nature and include *short-* and *long-range interactions* [12,15]. The long-range hydrodynamic interaction results as a fiber is placed in the disturbance flow field of other fibers. This type of interaction increases with the fiber concentration in the dilute and semi-dilute regimes but decreases in the concentrated regimes due to the screening effect that attenuates the disturbance. The short-range hydrodynamic interaction is due to the lubrication forces and torques that develop when two fibers get very close to one another. This happens when the concentration increases. One important characteristic of hydrodynamic interactions is that they are *diffusive* [16-17]. The reason is that a fiber undergoing hydrodynamic interaction with another fiber experiences a small displacement. For sufficiently large time intervals, this fiber experiences a large number of these displacements which are random in nature, and therefore the motion of its center of mass can be considered to undergo a diffusive process.

Finally, at high concentrations, mechanical interactions due to direct fiber-fiber contacts and Coulomb friction occur [13-14]. Physically, when the volume fraction exceeds the maximum

6

packing fraction of straight fibers, the fibers must bend elastically and exert contact normal forces on each other. When such a fiber network deforms, the fibers slide against one another, and friction forces are then produced. There have been a few micromechanical analyses of contacts with friction between two fibers that establish the forces resulting from these mechanisms [14,18]. Micromechanical analyses were also explored in the numerical simulations of the fiber suspensions that considered contacts with or without friction between the fibers [19-20]. Since no experimental observations exist to evidence the effect of fiber-fiber contact on the resulting composite microstructure, these simulations were very helpful to the understanding of the mechanical interactions and how they affect the rheological properties and composite microstructure.

It is noted that the relative importance of the mechanical and hydrodynamic interactions in controlling the microstructure of the suspension has not been clearly understood. Some authors considered that mechanical interactions are the dominant mechanism at high concentrations and then neglected the hydrodynamic interactions [19-20]. Sundararajakumar and Koch [19] carried out numerical simulations of sheared fiber suspensions containing a significant number of fibers (up to 60000 fibers) in a periodic simulation cell. These authors suggested that when the fiber concentration increases, hydrodynamic and mechanical interactions have a synergistic effect as each mechanism increases the orientation dispersion. At very high concentrations where each fiber can have several mechanical contacts, mechanical interactions are expected to dominate over hydrodynamic interactions. Sundararajakumar and Koch also have found that mechanical contacts enhance the shear viscosity of the suspension significantly. With the same type of approach, Switzer and Klingenberg [20] incorporated some realistic features of a fiber suspension such as fiber flexibility, irregular fiber shapes, friction and contacts into their dynamical simulation of the fiber suspension. They evidenced the flocculation (formation of heterogeneous distributions of mass) due to the fiber interlocking mechanism that can occur for a given concentration, fiber flexibility, and friction coefficient. Non-straight and stiff fibers in contact with high friction lead to flocculation. Although the mechanical interactions have been recognized as important mechanisms in concentrated suspensions, currently, there are no continuum models that incorporate these mechanisms into the fiber orientation equation.

Depending on the concentration regimes, both hydrodynamic and mechanical interactions do occur in SFT and LFT systems. For SFTs, Folgar and Tucker [4] added a diffusion term to the Jeffrey's dilute solution in order to represent the randomizing effect of the fiber-fiber interaction in concentrated suspensions. This term hence depicts the hydrodynamic interactions. Later, Advani and Tucker [5] recast the Folgar-Tucker equation in terms of the fiber orientation tensor components as:

$$\frac{DA_{ij}}{Dt} + \frac{1}{2}(\omega_{ik}A_{kj} - A_{ik}\omega_{kj}) = \frac{1}{2}\kappa(\dot{\gamma}_{ik}A_{kj} + A_{ik}\dot{\gamma}_{kj} - 2\dot{\gamma}_{kl}A_{ijkl}) + 2C_1\dot{\gamma}(\delta_{ij} - 3A_{ij}) \qquad (11)$$

where A_{ij} and A_{ijkl} are the second and fourth-order orientation tensors, respectively. ω_{ij} is the vorticity tensor, and $\dot{\gamma}_{ij}$ is the rate of the deformation tensor whose scalar magnitude is $\dot{\gamma}$. κ and C_1 are material constants; κ depends on the fiber aspect ratio r, and C_1 is called the interaction coefficient. If $C_1 = 0$ and, $\kappa = (r^2 - 1)/(r^2 + 1)$, Equation (11) is then Jeffrey's equation for the

motion of a rigid ellipsoidal shape fiber in a Newtonian solvent. This is strictly valid for dilute suspensions in which the fiber-fiber interaction is absent or negligible. C_I can be identified by fitting the predicted orientation results for the component a_{11} to the corresponding experimental data. Bay [21] has identified C_I for a set of short-glass fiber thermoplastics and has found that C_I initially increases as the fiber volume fraction or aspect ratio increases but beyond a certain value of cr ($cr > 1$, where c is the concentration), C_I decreases with increasing concentration. This can be explained by considering the screening effect that attenuates the disturbance at higher concentrations. The disturbance induced by the presence of a fiber is screened by the other fibers resulting in decreasing the fiber-fiber interaction, hence decreasing C_I. On the other hand, Phan-Thien et al. [22] have determined C_I as a function of cr by means of fiber suspension numerical simulations in which both short- and long-range hydrodynamic interactions were accounted for, and the suspending liquid was assumed to be Newtonian. They have found that C_I increases as a function of cr. Their findings, that do not agree with Bay's results for $cr > 1$, reveal the difficulty of obtaining C_I for high concentrations. Our recent numerical results (presented in the next Section) indicate that values C_I for LFTs are higher than those for SFTs.

Recent experience with SFTs suggests that the rate of orientation in concentrated fiber suspensions is slower than the standard model predicts (Eq. (11)), and thus the *SRF* (strain reduction factor) factor has been introduced to improve the agreement between prediction and experiment as [7]:

$$\frac{DA_{ij}}{Dt} + \frac{1}{2\,SRF}(\omega_{ik}A_{kj} - A_{ik}\omega_{kj}) = \frac{1}{SRF}[\frac{1}{2}\kappa(\dot{\gamma}_{ik}A_{kj} + A_{ik}\dot{\gamma}_{kj} - 2\dot{\gamma}_{kl}A_{ijkl}) + 2C_I\dot{\gamma}(\delta_{ij} - 3A_{ij})] \quad (12)$$

One problem arises in Equation (12) if SRF $\neq$ 1, namely it does not necessarily give the same answer in every coordinate system. To overcome this issue, in this report, a new model, called the *reduced strain closure RSC* model, was used that can be applied to all flows and coordinate systems. The RSC model is currently the subject of a patent application by the University of Illinois, so its details cannot be presented here. However, the performance of the RSC model in the flows simulated herein is very similar to Equation (12) with SRF > 1.

6. Rheological constitutive relation

A constitutive relation is necessary to relate the stress in the suspension to the rate of deformation, the fiber orientation state and the suspension parameters such as the fiber volume fraction, the fiber aspect ratio, and the viscosity of the suspending liquid. As the compressibilities of the suspending liquid and the fibers are negligible, the total stress is separated into an hydrostatic contribution from the pressure P plus a contribution from the suspension defined as the *extra stress*, τ_{ij} [1,3]:

$$\sigma_{ij} = -P\delta_{ij} + \tau_{ij} \quad (13)$$

In general, the extra stress includes the Newtonian contribution from the solvent, the stretching term that is proportional to the fourth-order orientation tensor, the shearing term containing the second-order orientation tensor, the contribution of the fibers, and the Brownian motion contribution. The last one is negligible for fiber suspensions. Also, the shearing term is much smaller than the stretching term for slender fibers. These simplifications lead to:

$$\tau_{ij} = 2\eta(\dot{\gamma},T)\,\dot{\gamma}_{ij} + 2\eta(\dot{\gamma},T)\,N_p\,a_{ijkl}\,\dot{\gamma}_{kl} \tag{14}$$

where $\eta = \eta(\dot{\gamma},T)$ is the suspension viscosity which is in general a strain rate and temperature-dependent material function. N_p is defined as the particle number and is a dimensionless parameter dependent on the fiber volume fraction and aspect ratio. Equation (14) expresses a strong dependence of the suspension rheology on the orientation state. Since fibers orient in response to the flow, and the suspension rheology depends on the fiber orientation, flow and orientation are strongly coupled. If N_p is equal to zero, Equation (14) is the constitutive relation of a generalized Newtonian fluid in which the stress field is assumed not to be dependent on the orientation state. This is the assumption for using a decoupled flow/orientation approach.

There have been attempts to improve the constitutive relation (14) to treat concentrated regimes [23], to include fiber-fiber interaction mechanisms [15], [24], and to address the non-Newtonian behavior of the suspending liquid e.g. [25]. Phan-Thien and Graham [23] introduced an empirical function that depends on the fiber volume fraction and aspect ratio to account for an important increase in viscosity in concentrated suspensions. Shafeq and Fredricson [24] improved the orientation-dependent term of Equation (14) to capture long-range hydrodynamic interaction while Moghaddam and Toll [15] extended the Shafeq-Fredricson model to include short-range hydrodynamic interaction. Certain fluids such as concentrated suspensions also exhibit yield phenomena in a similar way to ductile solids except that, at the onset of yield, the fluid will undergo viscous flow rather than plastic deformation. Thomasset et al. [25] combined the Oldroyd constitutive relation (that incorporated a yield stress) with the Carreau model for polymer viscosity to derive expressions for suspension shear and elongational viscosities. These authors have found that the suspension viscosities increase with fiber length and concentration, and with a greater important increase in elongational viscosity than in shear viscosity. Although different attempts have been made to improve the constitutive relation, the validation and application of these models are still limited to the studies of simple flows in order to investigate the effects of fiber concentration and length on the suspension viscosity. Also, the drawback of these models is that they introduce a significant number of empirical parameters that need to be identified. To date, the constitutive relation (14) remains the most efficient for engineering applications. The next section will review the coupled and decoupled flow/orientation approach.

7. Coupled and decoupled flow/orientation approaches

In general, flow and orientation are coupled since fibers orient in response to flow, and flow and suspension rheology are affected by fiber orientation. However, there are common cases of injection molding that involve flows in narrow gaps in which a decoupled flow/orientation approach is justified. Tucker [26] examined flow of fiber suspensions in narrow gaps using the constitutive relation (14), the fiber orientation equation (11), and scaling argument to simply the governing equations. Four distinct regimes of flow were then identified:

i. Decoupled lubrication flow: $\quad N_p \delta^2 \ll 1$ and $\delta \sim \varepsilon$

ii. Coupled lubrication flow: $\quad N_p \delta^2 \geq 1$ and $\varepsilon \ll \delta \ll 1$

iii. General narrow gap flow: $\quad N_p \delta^2 \gg 1$ and $\varepsilon \sim \delta$

iv. Plug flow with shear boundary layer: $\quad N_p \delta^2 \ll 1$ and $\delta \ll \varepsilon$

where δ describes the out-of-plane fiber orientation, and ε is the slenderness of the gap defined as *W/H* (*W* is typical dimension in the 1-2 plane which is the mid-plane between two surfaces defining the gap, and *H* is the gap height). The gap is narrow if ε is much less than unity. We are interested in regimes 1 and 2 in this work. In regime 1, the very small value of $N_p \delta^2$ means that the stretch rate along the fiber axes is so small and the fiber orientation is so flat, the fibers do not contribute to the gap-wise shear stresses. As a consequence, the orientation state does not appear in the momentum balance, and orientation is then *decoupled* from flow. In the second regime, $N_p \delta^2$ is near unity, the contribution of the particles to the viscosity cannot be neglected, and therefore, flow and fiber orientation are coupled. Injection molded parts possess some regions with complex geometry such as gate, rips, corners, etc. that may need a coupled flow/orientation analysis.

In a decoupled approach, the fluid flow problem is first solved as if the fibers were not present, and the resulting kinematics (i.e. velocity field) is used to compute the fiber orientation. On the other hand, in a coupled problem the flow and orientation equations must be solved simultaneously. Figure 1 gives a schematic description of the coupled and decoupled approaches based on Ranganathan and Advani [3]. These authors used this scheme to solve the flow and fiber orientation equation for an axisymmetric diverging radial flow using a finite difference method. In their decoupled approach, the flow field is calculated based on the rheology of the suspending fluid, the geometry of the flow field and the boundary conditions. Subsequently, the orientation equation (8) is used to determine the orientation state at various locations in the flow field. On the other hand, in the coupled problem illustrated in Figure 1, an iterative solution technique is required. The Newtonian flow solution is obtained first by neglecting the presence of fibers. The orientation state is computed based on this flow field. Using these orientation states, the rheological properties of the suspension are reevaluated at all the nodal points of the computational domain. The flow field is then recalculated with newly estimated rheological properties. This procedure is repeated until convergence of the flow field and fiber orientation state.

Recently, VerWeyst and Tucker proposed a finite element solution for the flow/orientation problem [27]. These authors formed a single set of discretized governing equations and solved them simultaneously using the Newton-Raphson method. The VerWeyst-Tucker method is more robust than the method employed by Ranganathan and Advani that used a finite difference technique. To date the coupled approach has not been implemented in commercial finite element software packages. In view of the computational time that this approach necessitates, its practical use for engineering applications has not been justified yet.
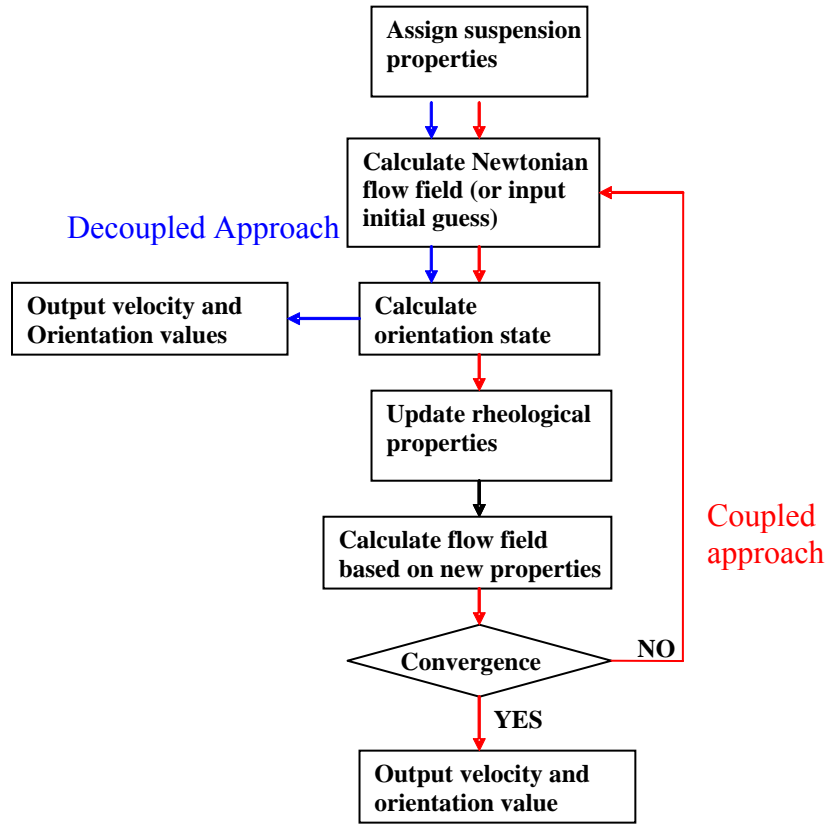
Figure 1. Decoupled and coupled flow/orientation approaches based on [3].

8. Model assessment

This section applies the current capabilities to computationally predict fiber orientation for three different LFT materials, using two different mold geometries: an end-gated strip and a center-gated disk. In order to compute the orientation state for an injection molding operation, the equations of balance of mass, momentum, and energy must be solved so that a velocity field can be computed. A program named ORIENT developed by the University of Illinois was used to solve for the velocity profile and the orientation in the above-mentioned geometries. A detailed description of the theory and numerical methods behind this program is found in [28]. ORIENT uses the Hele-Shaw approximation for solving for the velocity field in mold-filling operations where the velocity solution is decoupled from the orientation solution.

Table 1 provides a concise summary of each of the samples molded. The sample code identifies each material as "PNNLwxyz." The letter "w" identifies each material; "x" indicates either fast or slow injection speeds; y corresponds to the sample thickness in mm (all samples with orientation measurements were 3 mm thick at the time of this report); and z is indicates the part geometry (D or I, indicating a disk or ISO plaque). Material A has a polypropylene matrix with a 40% weight fraction of glass fibers. Material B is a polypropylene matrix with 31%

11

weight fraction of carbon fibers, and material C is the same as material B, with the exception that the carbon fibers are Nickel-coated. The center-gated disk is 177.8 mm in diameter, while the ISO plaque is 90 mm long and 80 mm wide. In each of the samples, the mold temperature was held to approximately 70 °C, and the inlet temperature of the melt was 238 °C.

8.1 Material properties:

Moldflow, Inc (Ithaca, NY) performed a complete evaluation of materials A and C and supplied the appropriate rheological and thermal properties. The properties of material B were assumed to be equivalent to those of material C. The density of material A was reported as 1.2203 g/cm^3, while materials B and C had a density of 0.9363 g/cm^3. Tables 2 and 3 give the specific heats c_p and thermal conductivities k, respectively, for each material over a range of temperatures. The viscosity of each material was reported to obey a Cross-WLF relationship with respect to strain rate and temperature, and the appropriate parameters were also calculated and reported by Moldflow. With this relationship, the viscosity η is related to the strain rate $\dot{\gamma}$ (i.e., the scalar magnitude of the rate-of-deformation tensor) through the Cross-WLF model which is

$$\eta = \eta_0 \left[1 + \left(\frac{\eta_0 \dot{\gamma}}{\tau *} \right)^{1-n} \right], \qquad (15)$$

where $\tau*$ and n are fitting parameters. This is a special case of the Cross-Carreau model. The WLF equation relates the reference viscosity η_0 to temperature T and is given as

$$\eta_0 = D_1 \exp \left[\frac{-A_1 (T - T*)}{A_2 + (T - T*)} \right], \qquad (16)$$

where D_1, A_1, and A_2 are fitting parameters and $T*$ is a reference temperature. Table 4 gives the fitting parameters for the Cross-WLF model for each material as reported by Moldflow. Figures 2 and 3 give plots of viscosity against strain rate at four temperatures for each material.

Table 1. Summary of materials, injection speed, and mold geometry for each of the samples examined in this report.

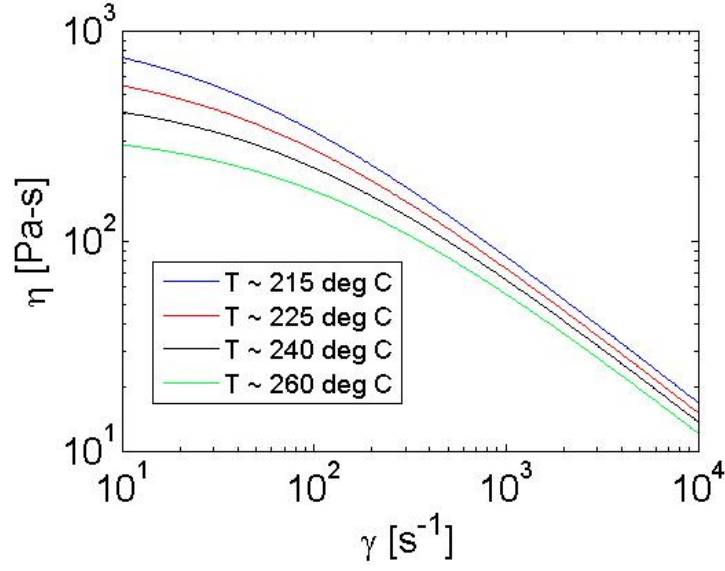| Sample Code	Material	Injection Speed Setting		Geometry
		Fill Speed	Fill Time [s]	
PNNLAF3D	A	Fast	0.65	Disk
PNNLAS3D	A	Slow	4.79-4.18	Disk
PNNLAF3I	A	Fast	0.48	ISO Plaque
PNNLAS3I	A	Slow	3.33	ISO Plaque
PNNLBF3D	B	Fast	0.67-0.81	Disk
PNNLBS3D	B	Slow	4.93-4.96	Disk
PNNLCF3D	C	Fast	0.67	Disk
PNNLCS3D	C	Slow	4.99-5.01	Disk
PNNLCF3I	C	Fast	0.475-0.480	ISO Plaque
PNNLCS3I	C	Slow	3.69-3.73	ISO Plaque

Figure 2. Viscosity η vs. strain rate $\dot{\gamma}$ for material A at four temperatures. Material A is a polypropylene composite with a 40% weight fraction of glass fibers.
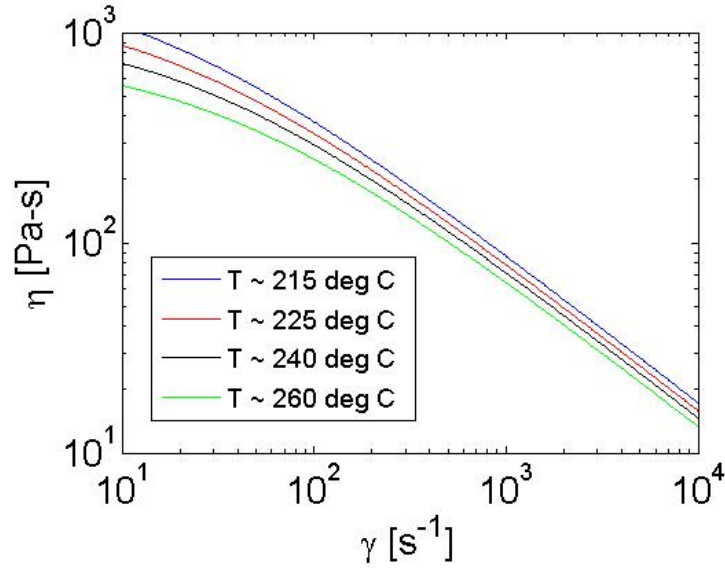

Figure 3. Viscosity η vs. strain rate $\dot{\gamma}$ for material B (or C) at four temperatures. Material B (or C) is a polypropylene composite with a 31% weight fraction of carbon (nickel-coated carbon) fibers.

Table 2. Specific heat c_p over a range of temperatures T for materials A, B and C as reported by Moldflow, Inc.

Material A		Material B (or C)	
T [°C]	c_p [J/kg-°C]	T [°C]	c_p [J/kg-°C]
260	2383.0	260	2299.0
135	2065.0	128	1964.0
125	2115.0	123	2370.0
121	3040.0	120	3669.0
118	5297.0	117	6319.0
115	14908.0	114	11472.0
112	6100.0	111	4102.0
109	2582.0	110	2911.0
100	2029.0	107	2126.0
75	1717.0	95	1815.0
60	1578.0	59	1426.0
50	1009.0	50	928.0

Table 3. Thermal conductivity k over a range of temperatures T for materials A, B and C as reported by Moldflow, Inc.

Material A		Material B (or C)	
T [°C]	k [W/m-°C]	T [°C]	k [W/m-°C]
260.6	0.197	260.5	0.320
239.1	0.188	239.7	0.316
218.1	0.181	218	0.256
198.4	0.188	198.2	0.302
178.3	0.193	178	0.288
157.5	0.197	157.4	0.297
137.1	0.174	138.5	0.417
117.8	0.252	118	0.406
97.4	0.252	97.4	0.399
77.2	0.232	77.6	0.404
57.6	0.240	57.7	0.393
38	0.259	37.9	0.379

Table 4. Fitting parameters for the Cross-WLF model for materials A, B, and C as reported by Moldflow.

Parameter	Material A	Material B (or C)
n	0.2768	0.2865
τ^* [Pa]	35922.1	26531.0
D_1 [Pa-s]	3.36477×10^{16}	5.68148×10^{13}
T^* [K]	263.15	263.15
A_1	38.390	29.764
A_2 [K]	51.600	51.600

8.2 Comparison method:

In order to compare the predicted and measured orientations, each of the samples presented in Table 1 were analyzed at three regions denoted A, B, and C. For the ISO plaques, region A was centered near the inlet at x = 15 mm, region B was centered approximately half-way down the length of the plaque at x = 45 mm, and region C was closer to the end of the plaque, centered at x = 75 mm. Each of the regions was located centrally in the cross-flow direction. For the center-gated disk, region A was located near the inlet at r = 6 mm, region B was at r = 34 mm, and region C was closer to the edge of the disk at r = 64 mm, where r is the radius of the disk. Each of the samples was 3 mm thick. The measured orientation data was computed at 21 slices across the thickness of the part.

Orientation measurements were preformed by ORNL staff at GM using a Leeds image analysis system developed by Hine et al. [29]. The important orientation descriptors are the orientation tensor elements A_{11}, A_{22}, A_{33}, and A_{31}. A_{11}, A_{22}, and A_{33} range between 0 and 1. For instance, a high value of A_{11} at a given point would indicate a great deal of orientation in the flow (x) direction. Similarly, a near-zero value of A_{33} would indicate little or no orientation in the thickness direction. On the other hand, A_{31} ranges between -0.5 and 0.5. In the x-z plane, a value of A_{31} approaching 0.5, would indicate high alignment in the direction 45° to the symmetry plane, whereas a value of A_{31} approaching -0.5 would indicate high alignment in the direction -45° to the symmetry plane.

ORIENT assumes symmetry about the mid-plane in the thickness direction, and this is reflected in the orientation predictions: the predicted values of A_{11}, A_{22}, and A_{33} are all symmetric about $z = 0$, while A_{31} is anti-symmetric about $z = 0$. The finite difference mesh used in ORIENT consisted of twenty-one nodes in the thickness direction and 121 nodes in the flow-direction. Region A corresponded to the 21st column of nodes in the flow direction, region B to the 61st column, and region C to the 101st column. Thus, at each region A, B, or C, ORIENT predicts the orientation tensor components for twenty-one points in the half-thickness of the piece.

8.3 Results:

For the results discussed in this section, all data have been taken at region B. At region A, there is little orientation development beyond the mold inlet, and since experimental data from region A was used for determining the inlet boundary condition for the ORIENT calculations, the predictions (not surprisingly) match the experimental data well in this region. In region C some samples exhibit significant orientation development beyond region B, but the qualitative description of the results remains the same as that for region B.

In the first samples examined, a determination regarding the model-experimental data fit was made. For material A in a fast-filled ISO plaque (PNNLAF3I), Figure 4 provides the A_{11} components of the second-order orientation tensor at region B as a function of the non-dimensional thickness coordinate z/b, where b is the half-thickness of the sample. Experiments show low alignment in the shell (the region near the mold walls) compared to short-fiber thermoplastics, which typically have shell-region A_{11} values close to 0.8. Also, a very thick core region (the region near the center of the sample with the lowest flow-direction orientation) was readily apparent. Applying a fiber interaction coefficient of 0.006 (typical for SFTs) to the model results in a poor fit to both the shell-region alignment and the thickness of the core. Increasing the fiber interaction coefficient better captures the shell-region alignment, but does not capture the wide core. Increasing the strain reduction factor (implementing the proprietary RSC model) and keeping the large C_I value can reasonably predict the shell-region alignment and the thick core. After several model iterations, it was determined that *a fiber interaction coefficient of 0.03 combined with a SRF>1 within the RSC model provided superior predicted results*.

Implementing the RSC model with an SRF factor of 30 and keeping $C_I = 0.03$ provides a good fit of the A_{11} tensor component for all glass fiber samples considered, regardless of fill speed or mold geometry. Thus, one set of fitting parameters are sufficient for each of the glass fiber-reinforced moldings in these trials. This is a significant finding resulting from our work. Figures 5-8 illustrate the A_{11} tensor component at region B for all glass fiber samples. However, using the parameters described previously under-predicts the value of A_{22}. By extension, A_{33} is over-predicted, since the trace of A equals unity. As an example, Figure 9 gives A_{22} and A_{33} for a slow-filled glass fiber ISO plaque (PNNLAS3I). In general, A_{31} is poorly fit for all samples considered.

In comparing only experimental data, Figure 10 shows the difference in the A_{11} orientation tensor component between the three materials for a slow-fill disk. Material A (40% fiber weight fraction of glass fibers) and material B (31% fiber weight fraction of carbon fibers) exhibit similar behavior near the core, but material A shows strong asymmetry about the mid-plane. Material C (31% fiber weight fraction of Ni-coated carbon fibers) exhibits much less flow-direction alignment than the other materials and has a thicker core.

By increasing the *SRF* factor to 50 and keeping $C_I = 0.03$, a reasonable fit to A_{11} is achieved for the uncoated carbon fiber samples. Figures 11 and 12 give A_{11} vs. *z/b* for the uncoated carbon fiber fast-fill and slow-fill disks. No experimental data was reported for uncoated carbon fiber ISO plaques. The same set of parameters gives the best fit to the Ni-coated carbon fiber samples as well. However, with the coated carbon fibers, the overall lower alignment in the shell and core regions makes for more difficult fitting. Figures 13-16 give A_{11} against the non-dimensional thickness coordinate for the fast-filled and slow filled ISO plaques and disks. The under-prediction in A_{22} and over-prediction in A_{33} are the same as those seen in the glass fiber samples.

9. Conclusions

A thorough technical assessment of the current process modeling approaches has been conducted in this study leading to the following conclusions:

- The current fiber orientation and constitutive models can adequately predict the fiber orientation, suspension viscosity in dilute and semi-concentrated regimes. However, these models have limitations to capture the fiber orientation in concentrated regimes. This is true for both short- or long-fiber systems.

- The Hele-Shaw assumption for flows in thin cavities applies to both short- and long-fiber systems.

- Recent improvement of the Folgar-Tucker model leading to the RSC model is a significant step to address the fiber orientation in LFTs. However, only qualitative agreement has been found with the experimental results measured with the Leeds system. The validation of the Leeds results has just been achieved by the University of Illinois at Urbana-Champaign by means of manual fiber orientation measurement for some selected LFT samples studied in Section 8 (i.e. glass, carbon and Ni-coated carbon fiber-PP center-gated disks and ISO-plaques).This validation work shows that there have been good agreements between the Leeds results and the orientation data obtained by manual measurement. Therefore, the validity of the Leeds results for the studied LFT samples has been confirmed. It has been noted that the flow-direction alignment in the LFT shell layers is much lower than expected.

- The best fits of the RSC model to LFT fiber orientation data show that the SRF value for carbon fibers is higher than the SRF value for glass fibers. This suggests that fiber stiffness plays a role in determining SRF.

- Neither the standard fiber orientation model nor the new RSC model can predict fiber orientation in LFT samples to the level of accuracy needed for predictive engineering.

- The fundamental limitation of the fiber orientation model seems to reside in the interaction term. This term needs to be improved to account for the rotation of long fibers and the anisotropic character of the fiber-fiber interaction which cannot be adequately represented by an isotropic rotary diffusion term. Efforts have been being taken to incorporate an anisotropic rotary diffusion term to model the fiber orientation in LFTs.
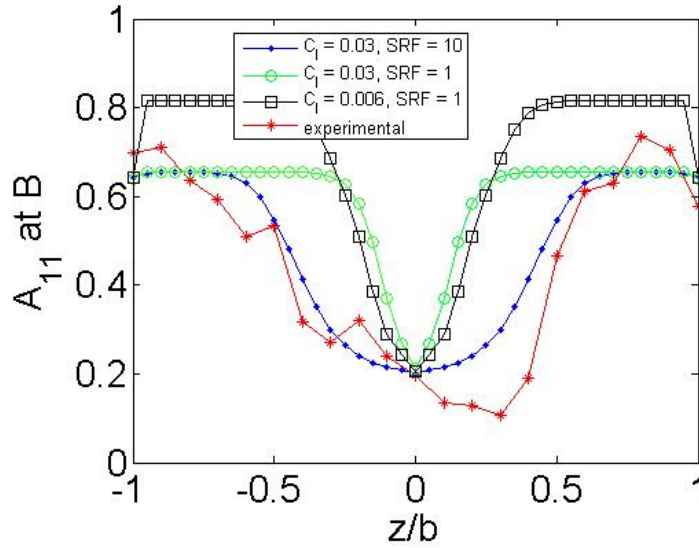
10. Acknowledgements

Figure 4. A_{11} vs. non-dimensional thickness coordinate z/b for PNNLAF3I. The experimental data is compared against three different sets of parameters for orientation modeling. The best fit is provided by the RSC model with a *SRF* factor much greater than one and $C_I = 0.03$.
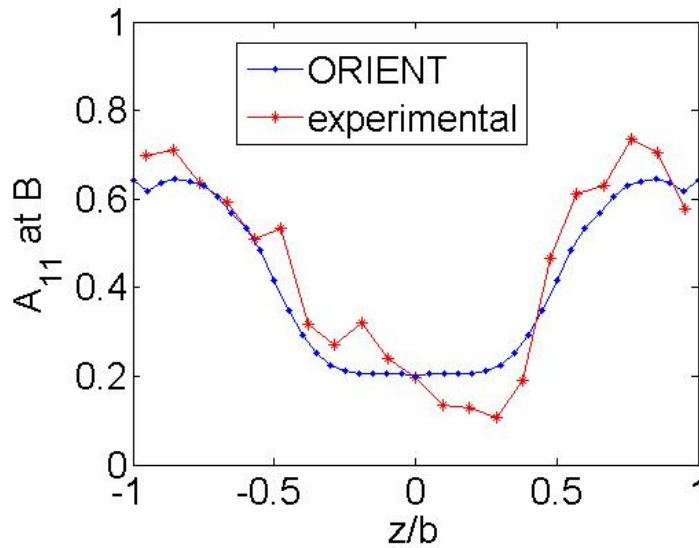

Figure 5. A_{11} vs. non-dimensional thickness coordinate z/b for PNNLAF3I at region B. *SRF* = 30 and $C_I = 0.03$.
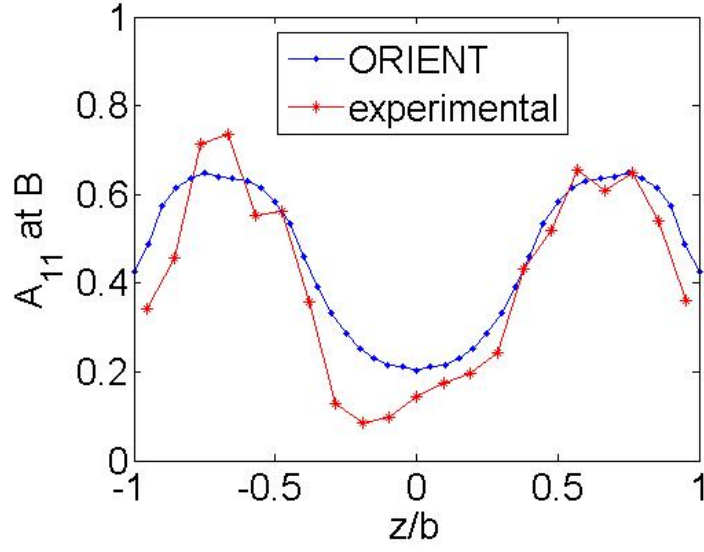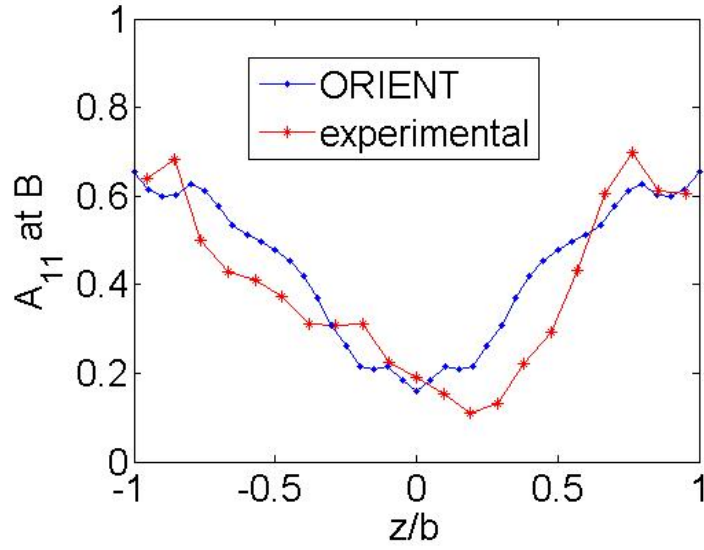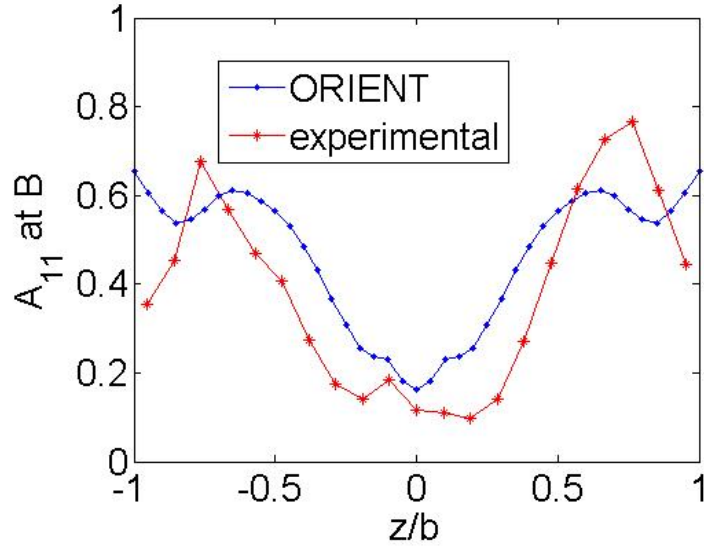
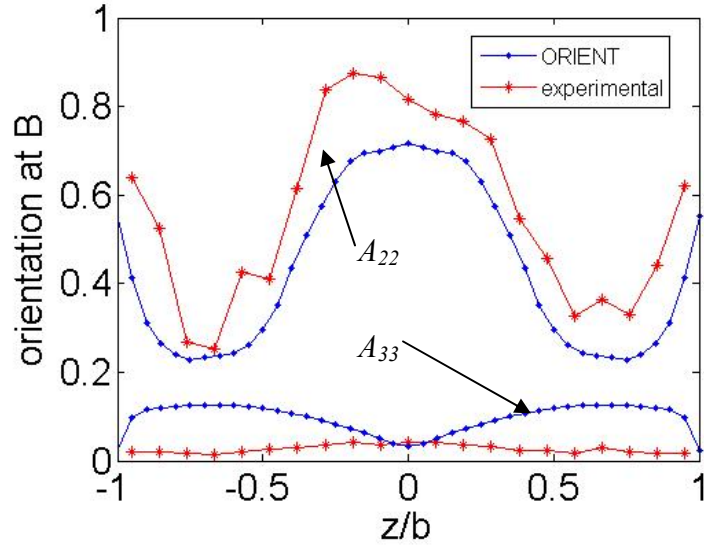**Figure 6.** A_{11} vs. non-dimensional thickness coordinate *z/b* for PNNLAS3I at region B. *SRF* = 30 and C_I = 0.03.

Figure 7. A_{11} vs. non-dimensional thickness coordinate *z/b* for PNNLAF3D at region B. *SRF* = 30 and C_I = 0.03.
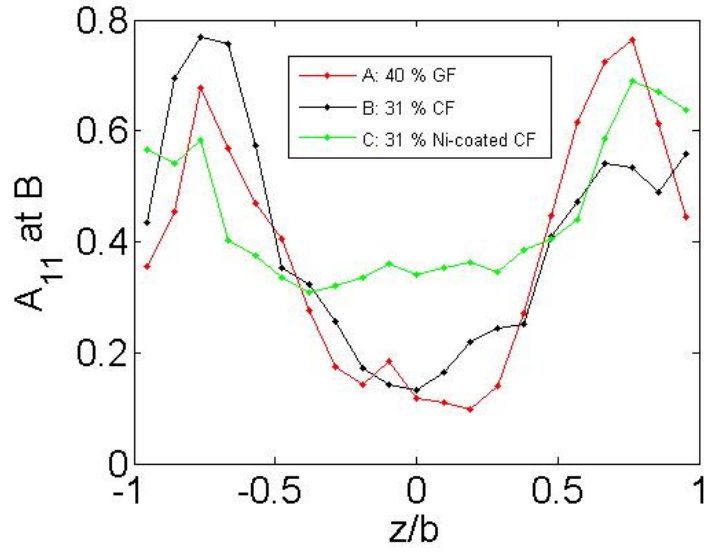
Figure 8. A_{11} vs. non-dimensional thickness coordinate *z/b* for PNNLAS3D at region B. *SRF* = 30 and C_I= 0.03.

Figure 9. A_{22} and A_{33} vs. non-dimensional thickness coordinate *z/b* for PNNLAS3I at region B. *SRF* = 30 and C_I= 0.03.

Figure 10. Experimental A_{11} vs. z/b at region B for all three materials. The samples were slow-filled disks.
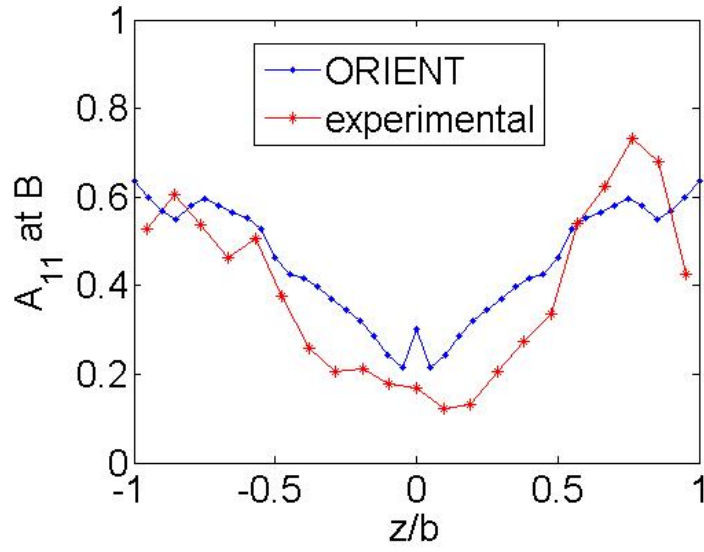

Figure 11. *A_{11}* vs. non-dimensional thickness coordinate *z/b* for PNNLBF3D at region B. *SRF =* 50 and *C_I* = 0.03.
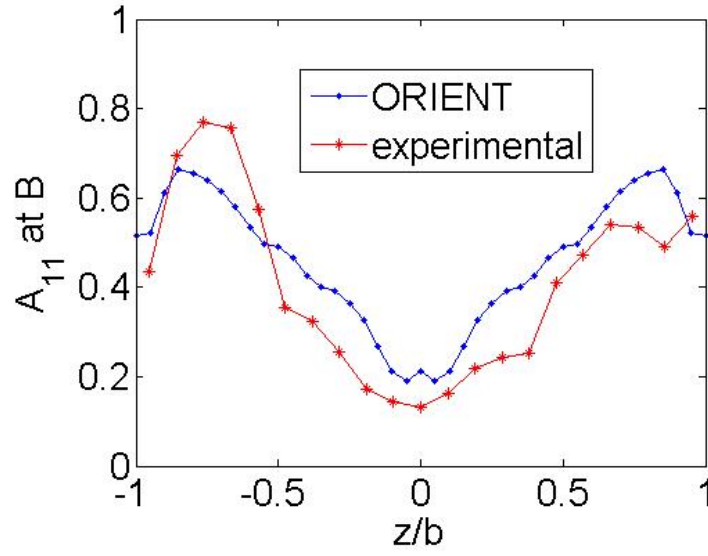
Figure 12. A_{11} vs. non-dimensional thickness coordinate z/b for PNNLBS3D at region B. *SRF* = 50 and C_I = 0.03.
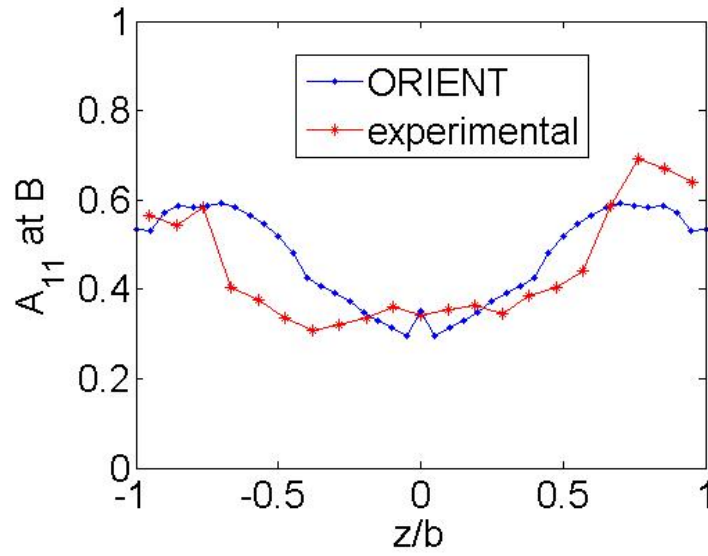

Figure 13. A_{11} vs. non-dimensional thickness coordinate z/b for PNNLCF3I at region B. *SRF* = 50 and C_I = 0.03.
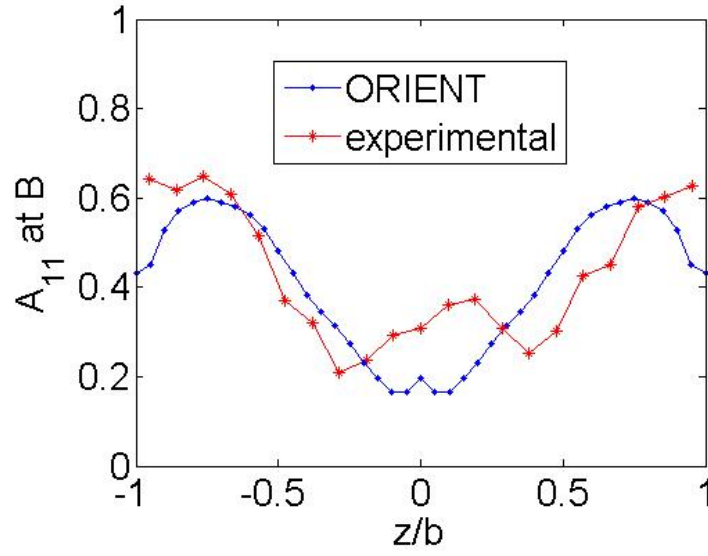
Figure 14. A_{11} vs. non-dimensional thickness coordinate z/b for PNNLCS3I at region B. *SRF* = 50 and C_I = 0.03.
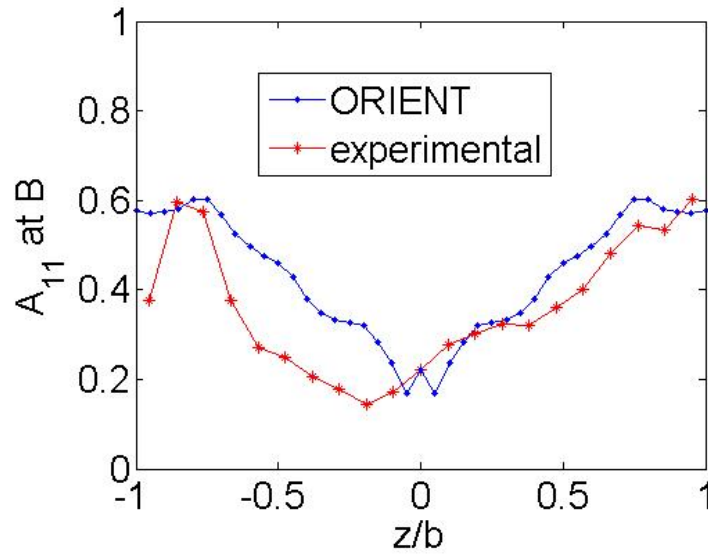

Figure 15. A_{11} vs. non-dimensional thickness coordinate z/b for PNNLCF3D at region B. *SRF* = 50 and C_I = 0.03.
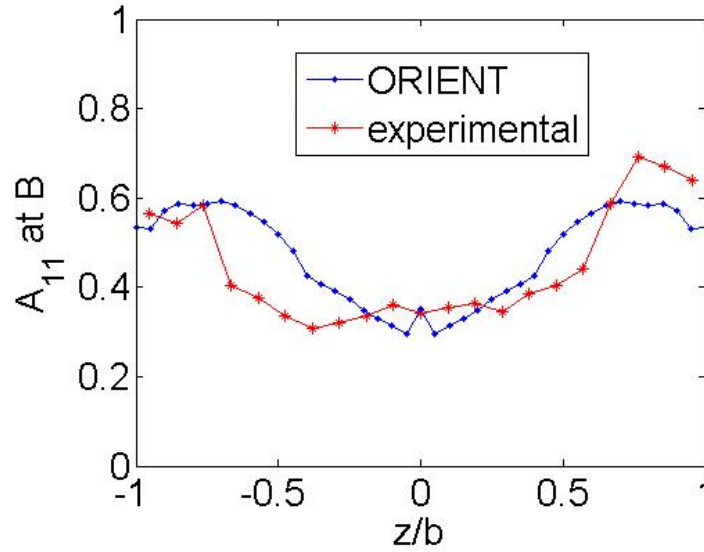
Figure 16. A_{11} vs. non-dimensional thickness coordinate z/b for PNNLCS3D at region B. *SRF* = 50 and C_I = 0.03.

References

1. C.L. Tucker III and S.G. Advani (1994). "Processing of Short-Fiber Systems." In: Flow and Rheology in Polymer Composites Manufacturing, S.G. Advani, Ed., Elsevier Science, 147-202.
2. C.C. Lee, F. Folgar, and C.L. Tucker III (1984). "Simulation of Compression Molding for Fiber Reinforced Thermosetting Polymers," Journal of Engineering Industry, 106, 114-125.
3. S. Ranganathan and S.G. Advani (1993). "A Simultaneous Solution for Flow and Fiber orientation in Axisymmetric Diverging Radial Flow," Journal of Non-Newtonian Fluid Mechanics, 47, 107-136.
4. F. Folgar and C.L. Tucker III (1984). "Orientation Behavior of Fibers in Concentrated Suspensions," Journal of Reinforced Plastic Composites, 3, 98-119.
5. S.G. Advani and C.L. Tucker III (1987). "The Use of Tensors to Describe and Predict Fiber Orientation in Short-Fiber Composites," Journal of Rheology, 31 (8), 751-784.
6. S. Ranganathan and S.G. Advani (1997). "Fiber-Fiber and Fiber-Wall Interactions during the Flow of Non-Dilute Suspensions." In: Flow-Induced Alignment in Composite Materials, T.D. Papathanasiou & D.C. Guell, Eds, Woodhead Publishing Ltd, 43-76.
7. H. M. Huynh (1999). Improved fiber orientation predictions for injection-molded composites. Master's thesis, University of Illinois, Urbana, IL.
8. J.H. Phelps and C.L. Tucker III (2006). "Assessing Fiber Orientation Prediction Capability for Long-Fiber Thermoplastic Composites." Technical Report submitted to PNNL, University of Illinois at Urbana-Champaign.

9. M.J. Crochet, F. Dupret and V. Verleye (1994). "Injection Molding." in: Flow and Rheology in Polymer Composites Manufacturing, S.G. Advani, Ed., Elsevier Science, 415-463.

10. T.D. Papathanasiou (1997). "Flow-Induced Alignment in Injection Molding of Fiber-Reinforced Polymer Composites." In: Flow-Induced Alignment in Composite Materials, T.D. Papathanasiou & D.C. Guell, Eds, Woodhead Publishing Ltd, 112-165.

11. Jeffrey, G. B. (1922). "The Motion of Ellipsoidal Particles Immersed in Viscous Fluid", Proceedings of the Royal Society London, A102, 161-179.

12. M. Rahnama, D.L. Koch, and E.S.G. Shaqfeh (1995). "The Effect of Hydrodynamic Interactions on the Orientation Distribution in a Fiber Suspension Subject to Simple Shear Flow." Physics of Fluids, 7(3), 487-506.

13. C. Servais, J.-A. E. Manson, and S. Toll (1999). "Fiber-Fiber Interaction in Concentrated Suspensions : Disperse Fibers." Journal of Rheology, 43(4), 991-997.

14. S. Toll and J.-A. E. Manson (1994). "Dynamics of a Planar Concentrated Fiber Suspension with Non-hydrodynamic Interaction." Journal of Rheology, 38(4), 985-997.

15. M. Djalili-Moghaddam and S. Toll (2005). "A Model for Short-Range Interactions in Fiber Suspensions." Journal of Non-Newtonian Fluid Mechanics, 132, 73-83.

16. D.L. Koch (1995). "A Model for Orientational Diffusion in Fiber Suspensions." (Brief Communications), Physics of Fluids, 7(8), 2086-2088.

17. M. Rahnama, D.L. Koch, Y. Iso, and C. Cohen (1993). "Hydrodynamics, Translational Diffusion in Fiber Suspension Subject to Simple Shear Flow." Physics of Fluids A, 5(4), 849-862.

18. M.P. Petrich and D.L. Koch (1998). "Interactions between Contacting Fibers." Physics of Fluids, 10(8), 2111-2113.

19. R.R. Sundararajakumar and D.L. Koch (1997). "Structure and Properties of Sheared Fiber Suspensions with Mechanical Contacts." Journal of Non-Newtonian Fluid Mechanics, 73, 205-239.

20. L.H. Switzer and D.J. Klingenberg (2003). "Flocculation in Simulations of Sheared Fiber Suspensions." International Journal of Multiphase Flow, 30, 67-87.

21. R.S. Bay (1991). "Fiber Orientation in Injection Molded Composites: A Comparison of Theory and Experiment." Ph.D. Thesis, Department of Mechanical Engineering, University of Illinois, Urbana, Illinois.

22. N. Phan-Thien, X.J. Fan, R.I. Tanner, and R. Zheng (2002). "Folgar-Tucker Constant for a Fibre Suspension in a Newtonian Fluid." Journal of Non-Newtonian Fluid Mechanics, 103, 251-260 (Short communication).

23. N. Phan-Thien and A.L. Graham (1991). "A New Constitutive Model for Fiber Suspensions: Flow Past a Sphere." 30, 44-57.

24. E.S.G. Shaqfeh and G.H. Fredrickson (1990). "The Hydrodynamic Stress in Suspension of Rods." Physics of Fluids A, 2, 7-24.

25. J. Thomasset, P.J. Carreau, B. Sanschagrin, and G. Ausias (2005). "Rheological Properties of Long Glass Fiber Filled Polypropylene." Journal of Non-Newtonian Fluid Mechanics, 125, 25-34.

26. C.L. Tucker III (1991). "Flow Regimes for Fiber Suspensions in Narrow Gaps." Journal of Non-Newtonian Fluid Mechanics, 39, 239-268.

27. B.E. VerWeyst and C.L. Tucker III (2002). "Fiber Suspensions in Complex Geometries: Flow/Orientation Coupling." Canadian Journal of Chemical Engineering, 80(6), 1093-1106.

28. R. S. Bay and C. L. Tucker III (1992). "Fiber Orientation in Simple Injection Moldings. Part I: Theory and Numerical Methods. Polymer Composites, 13, 317-331.

29. P.J. Hine, N. Davidson, R. A. Duckett, A. R. Clarke, I. M. Ward (1996). "Hydrostatically Extruded Glass-Fiber-Reinforced Polyoxymethylene. I: The development of Fiber and Matrix Orientation." Polymer Composites. 17, 720-729.